Visible-light absorptivity of a zincoxysulfide ($ZnO_xS_{1−x}$) composite semiconductor and its photocatalytic activities for degradation of organic pollutants under visible-light irradiation

Cham Kim *, Seok Joo Doh, Se Geun Lee, Sung Jun Lee, Ho Young Kim

Advanced Nano Materials Research Team, Daegu Gyeongbuk Institute of Science and Technology (DGIST),
711-521 Hosan-dong, Dalseo-gu, Daegu 704-230, South Korea

Abstract

This work reports the development of a visible-light sensible photocatalyst and the photocatalytic degradation of organic pollutants under visible-light irradiation. A composite semiconductor of ZnS and ZnO was prepared through co-precipitation process of $Zn(NO_3)_2$ in the mixed solution of aqueous Na_2S and NaOH followed by calcination at 400 °C in N_2 atmosphere. It was revealed that the composite semiconductor was a solid solution of ZnS and ZnO, a zincoxysulfide ($ZnO_xS_{1−x}$) having advanced visible-light absorptivity. It was assured that the visible-light absorptivity was caused by modification of band structure while the solid solution had been prepared, thus we suggested a reasonable band structure model involved in a zincoxysulfide. To observe its photocatalytic activity under visible-light illumination, photodegradation test was done and we confirmed that zincoxysulfide showed predominant photocatalytic activity due to its superior visible-light absorptivity to pure ZnS and ZnO.
© 2007 Elsevier B.V. All rights reserved.

Keywords: Photocatalyst; Visible light; ZnS; ZnO; Zincoxysulfide ($ZnO_xS_{1−x}$)

1. Introduction

Recently, a lot of studies have been concentrated on the degradation of toxic organic compounds in wastewater via photocatalysis of various semiconductors [1–15]. For instance, TiO_2 with anatase phase has been most widely investigated due to its acceptable photocatalytic activity and chemical stability. However, it is generally known that TiO_2 can barely absorb visible light due to its wide band-gap energy (3.2 eV) and this is one of the most serious problems associated with its further applications [14–20].

To synthesize visible-light driven photocatalysts, some approaches have been suggested, and these are classified in three ways [21]. The first approach is doping various nonmetals into photocatalysts with wide band-gap energies to intercalate localized donor levels in the forbidden band. TiO_2 doped with diverse nonmetals, such as carbon [22–24], nitrogen [25–30],

and sulfur [31–33] are classified in the first approach. However, it has some drawbacks involved in discrete doping levels and low mobility of electrons and holes [21]. The second approach is building up valence band in a more negative position. $BiVO_4$ [34,35], TaON [36], and $(Ga_{1−x}Zn_x)(N_{1−x}O_x)$ [37] have been proven as visible-light sensible photocatalysts having valence bands composed of hybrid orbitals of Bi6s, N2p and (N2p + Zn3d) with O2p, respectively. The third approach is regulating band-gap energies by making a compound of two different semiconductors with wide and narrow band gaps. Various materials, such as SnO_2-TiO_2 [38], $Sr_2Nb_2O_7$-$Sr_2Ta_2O_7$ [39,40], and Nb_2O_5-Bi_2O_3 [41] have been reported showing visible-light response and it was known that their structural properties and photocatalytic activities were mainly influenced by their compositions.

Ishikawa et al. reported band-gap diminution by making a composite semiconductor, $Sm_2Ti_2S_2O_5$ including an oxysulfide [42]. They used Sm_2S_3, Sm_2O_3, and TiO_2 to synthesize the composite semiconductor. According to their report, top of the valence band of $Sm_2Ti_2S_2O_5$ is predominantly composed of S3p orbitals because they have higher potential energies than

* Corresponding author. Tel.: +82 53 430 8436; fax: +82 53 430 8443.
  E-mail address: charming0207@dgist.ac.kr (C. Kim).

those of O2p orbitals. Therefore, they verified that valence band of $Sm_2Ti_2S_2O_5$ has been formed in a more negative position than O2p, resulting in the small band gap. Namely, they insisted that the small band-gap energy of $Sm_2Ti_2S_2O_5$ should occur due to the hybrid orbitals of sulfur and oxygen caused by the formation of an oxysulfide.

Meanwhile, we adopted ZnS and ZnO in this study to gain a visible-light driven photocatalyst. We expected that they would be also able to have an oxysulfide when they constitute a composite semiconductor because sulfur exists as an anion (S^{2-}) in ZnS. Thus, the process to develop a visible-light sensible photocatalyst in this research is classified in the second approach and there have been no reports to apply the composite semiconductor of ZnS and ZnO as a visible-light sensible photocatalyst, to the best of our knowledge.

Consequently, we have developed the composite semiconductor of ZnS and ZnO having visible-light absorptivity through co-precipitation process and named it as 'zincoxysulfide (ZnO_xS_{1-x})'. We ascertained that band-gap diminution was possible when ZnS and ZnO has organized a composite resulted in the formation of an oxysulfide. In the present article, we report visible-light response of the zincoxysulfide resulted from band-gap modification and its photocatalytic activities for the degradation of organic pollutants under visible-light irradiation.

2. Experimental

2.1. Chemicals

Sodium sulfide (Na_2S, Acros, 60–62%), aqueous sodium hydroxide (NaOH, Samchun, 1 mol L^{-1}), and zinc nitrate ($Zn(NO_3)_2$, Kanto, 99%) were selected to synthesize the ZnO_xS_{1-x} composite. Pure zinc sulfide (ZnS, Wako, 99%) and zinc oxide (ZnO, Kanto, 99%) were also chosen to compare their structural and photocatalytic properties to those of the composite. A commercial dye, Basic Red 2 (Sigma–Aldrich, 99%) and a chlorinated phenol, 4-chlorocatechol (TCI, 99%) were adopted as model pollutants. They have maximum absorption wavelength at 520 and 284 nm, respectively, and their absorption patterns and chemical formulas are shown in Fig. 1. Water was deionized and doubly distilled with Milli-Q.

2.2. Procedures

ZnS and ZnO can be easily prepared by general precipitation method via Eqs. (1) and (2), respectively. Thus, we attempted to synthesize the ZnO_xS_{1-x} composite, which molar ratio between ZnS and ZnO is 1:3, through co-precipitation process of $Zn(NO_3)_2$ in the mixed solution of aqueous Na_2S and NaOH (Eq. (3)). The ratio can be easily controlled by altering the amount of Na_2S and NaOH solution.

$$Zn(NO_3)_2(aq) + Na_2S(aq) \rightarrow ZnS(s) + 2NaNO_3(aq) \qquad (1)$$

$$Zn(NO_3)_2(aq) + 2NaOH(aq) \rightarrow ZnO(s) + 2NaNO_3(aq) + H_2O(l) \qquad (2)$$
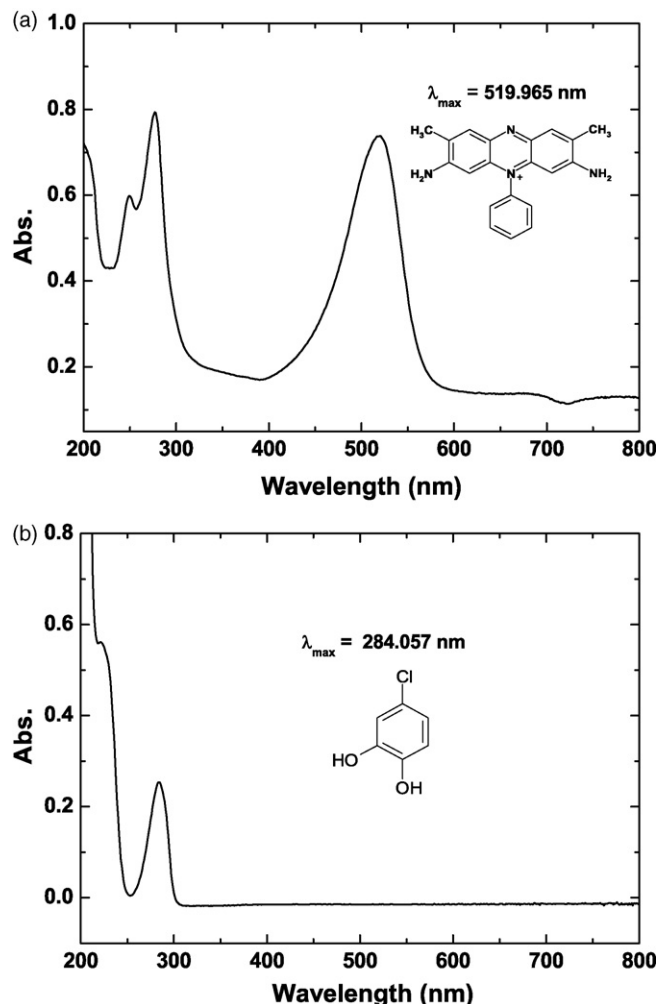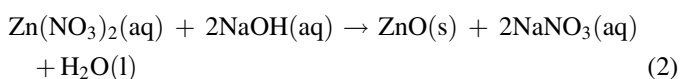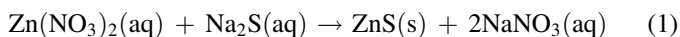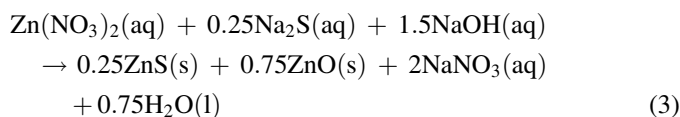

Fig. 1. Absorbance spectra, maximum absorption wavelengths, and structures of BR2 (a) and 4-CC (b).

$$Zn(NO_3)_2(aq) + 0.25Na_2S(aq) + 1.5NaOH(aq)$$
$$\rightarrow 0.25ZnS(s) + 0.75ZnO(s) + 2NaNO_3(aq)$$
$$+ 0.75H_2O(l) \qquad (3)$$

0.39 g of Na_2S, 30 mL of aqueous NaOH, and 10.66 g of $Zn(NO_3)_2$ were dissolved in 150, 100, and 50 mL of distilled water, respectively, and they were vigorously stirred for 1 h. The Na_2S solution was poured into the NaOH solution and stirred for 1 h, additionally (solution A). Then 30 mL of $Zn(NO_3)_2$ solution was slowly injected into the solution A with specific input rate using 50 mL syringe. Resulting precipitates were aged for 7 h, and then filtered through a 0.45 μm filter membrane (Millipore) followed by washing with deionized water. The precipitates were dried in a vacuum oven for overnight and calcined at 400 °C for 2 h with N_2 flow.

2.3. Photocatalytic treatment

All photodegradation experiments of Basic Red 2 (BR2, 1.43×10^{-5} mol L^{-1}) and 4-chlorocatechol (4-CC, 8×10^{-5} mol L^{-1}) were conducted in a batch reactor in this study. The
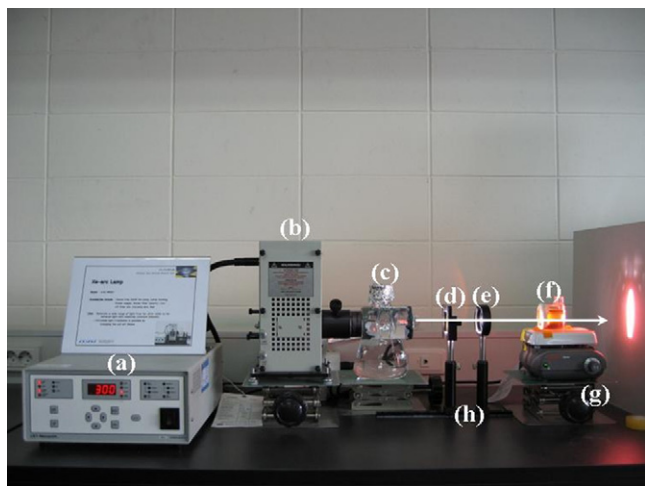
Fig. 2. Photocatalytic reactor. Power supply (a), lamp housing equipped with 300 W ozone-free Xe-arc lamp (b), water filter (quartz) (c), cut-off filter (d), focusing lens (e), batch reactor (f), stirrer (g), rail (h).

batch reactor, which is a 45 mm × 45 mm × 55 mm and 90 mL homemade cylindrical glass cell, has one perpendicular surface and light was illuminated to this surface to minimize light scattering. A 300 W ozone-free xenon-arc lamp (Newport), which can generate a wide range of light from far ultra-violet to far infrared light with relatively constant intensity, was adopted as a light source, and a cut-off filter (CVI) was used to intercept UV light ($\lambda \leq 400$ nm) and make visible light ($\lambda > 400$ nm) reach to the batch reactor (Fig. 2). Eighty milliliters of BR2 and 4-CC aqueous solutions without the photocatalysts were preferentially illuminated under visible light for 180 min to measure the amount of each pollutant decomposed only by the light irradiation. Each 0.08 g of ZnS, ZnO, and ZnO_xS_{1-x} was individually mixed with the BR2 or 4-CC aqueous solutions, and the mixtures were stirred for 30 min without the irradiation initially to consider the amount of each pollutant adsorbed on the surface of the photocatalysts. These mixtures were also irradiated for 180 min. All of the samples were extracted with a 3 mL syringe every single 30 min and filtered through a syringe-driven filter unit (0.45 μm, Millipore) to check out photodecomposition rate of BR2 or 4-CC during the light irradiation.

2.4. Characterization studies

Powder X-ray diffraction patterns of the photocatalysts were collected in a D/MAX-2500 diffractometer (Rigaku) using Cu Kα radiation and a scintillation counter detector. The patterns were recorded in the 2θ range of 20–80°. Field emission scanning electron micrographs were obtained by using a S-4800 FE-SEM (Hitachi) equipped with a detector for energy dispersive spectroscopy (EDS). X-ray photoelectron spectroscopy (XPS) was performed using VG EscaLab 220-IXL BASE SYSTEM (VG scientific) with Mg Kα radiation. The C1s photoelectron peak (binding energy at 284.6 eV) was used as energy reference. UV–vis diffuse reflectance spectra (DRS) were obtained from a Cary 5000 UV-Vis spectrophotometer (Varian) equipped with an internal diffuse reflectance

integrating sphere. The spectra were recorded in the range of 300–600 nm to confirm visible-light absorptivity of ZnS, ZnO, and ZnO_xS_{1-x}. The photocatalytic degradation of BR2 and 4-CC was observed by using a Cary 50 UV-Vis spectrophotometer (Varian).

3. Results and discussion

Fig. 3a highlights the comparison of XRD patterns among the photocatalysts. The patterns of pure ZnO showed a hexagonal wurtzite structure having diffraction lines of (1 0 0), (0 0 2), (1 0 1), (1 0 2), (1 1 0), (1 0 3), (2 0 0), (1 1 2), (2 0 1), (0 0 4), and (2 0 2) planes at 2θ values of 31.9°, 34.6°, 36.5°, 47.7°, 56.8°, 63.1°, 66.5°, 68.0°, 69.2°, 72.7°, and 77.1°, respectively, which coincide with the value of JCPDS Card No. 36-1451. Pure ZnS exhibited diffraction lines of (1 0 0), (0 0 2), (1 0 1), (1 0 2), (1 1 0), (1 0 3), (2 0 0), (1 1 2), (2 0 1), (0 0 4), (2 0 2), (1 0 4), (2 0 3), (2 1 0), (2 1 1), and (1 1 4) planes at 2θ values of 27.0°, 28.5°, 30.5°, 39.7°, 47.6°, 51.8°, 55.6°, 56.4°,
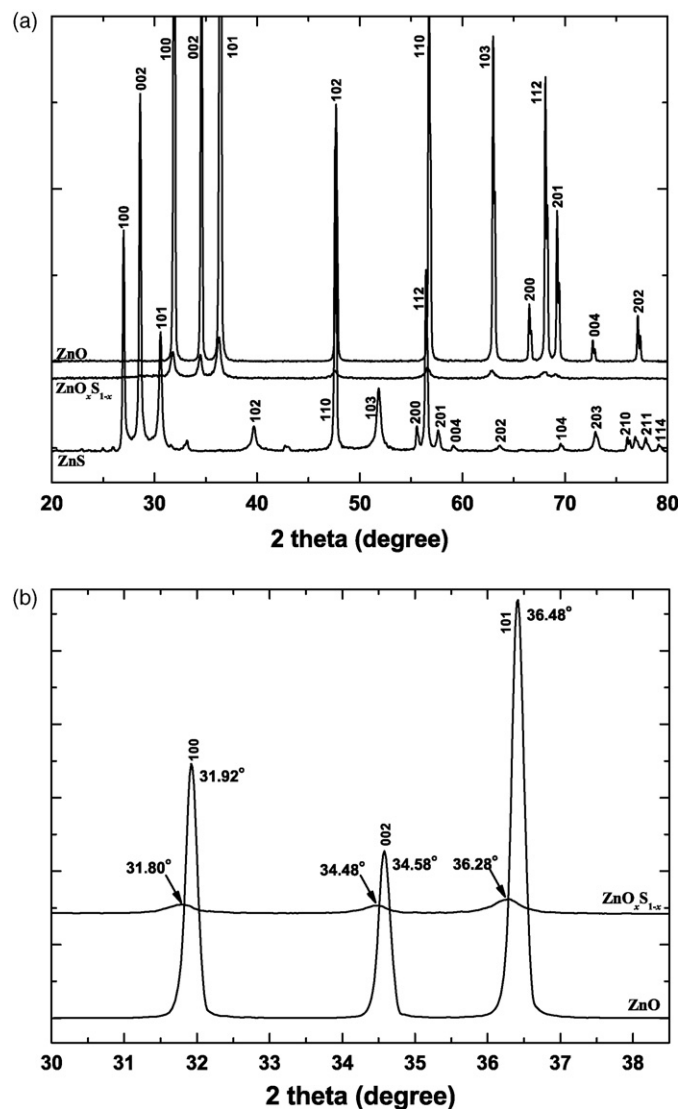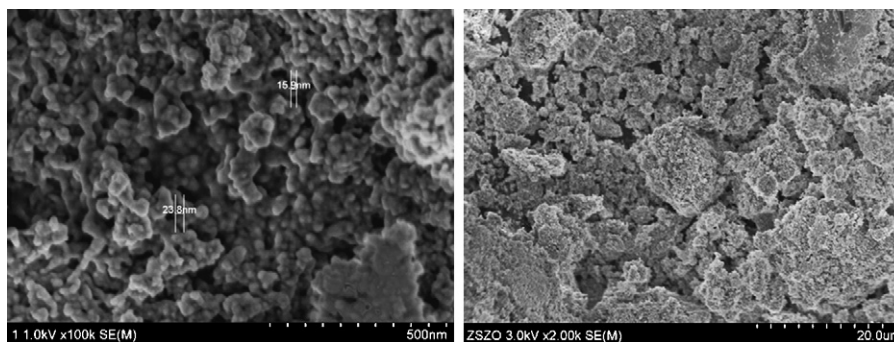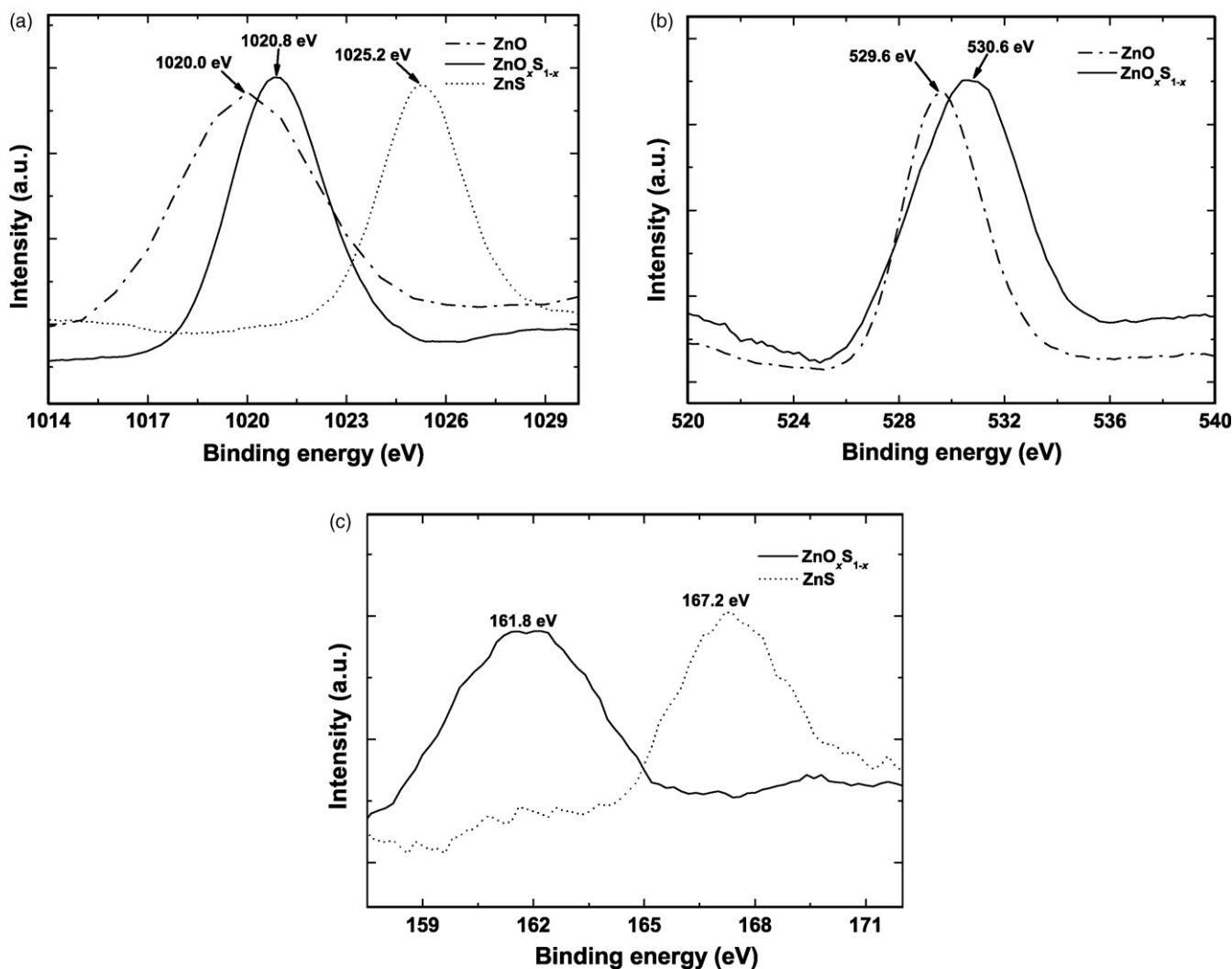

Fig. 3. X-ray diffraction patterns of ZnS, ZnO, and ZnO_xS_{1-x} (a), and comparison of diffraction patterns between ZnO and ZnO_xS_{1-x} (b).

Fig. 4. Scanning electron micrographs of ZnO_xS_{1-x}.

$57.6°$, $59.3°$, $63.4°$, $69.6°$, $72.9°$, $76.2°$, $77.8°$, and $79.2°$, respectively, indicating a typical hexagonal wurtzite structure, which is consistent with the value of JCPDS Card No. 36-1450. The composite of ZnS and ZnO also exhibited a hexagonal wurtzite structure and its diffraction pattern was very similar to one of ZnO. The diffraction lines of the composite were shifted to a lower angle side (Fig. 3b) and no diffraction lines of ZnS were found. According to the analysis of scanning electron micrograph for the composite shown in Fig. 4, it was verified that particles ranging from 15 to 25 nm have been formed. We confirmed that they were mostly composed of zinc, oxygen, and sulfur via energy dispersive spectra (EDS) (not shown). The results from XRD and EDS indicates that the obtained crystals are not the simple mixtures of ZnS and ZnO but their solid solutions. Therefore, we assumed that zinc should have chemical bonding to both sulfur and oxide and named it as zincoxysulfide (ZnO_xS_{1-x}).

Fig. 5. XPS spectra of $Zn2p_{3/2}$ (a), O1s (b), and S2p (c) for ZnS, ZnO, and ZnO_xS_{1-x}.

To confirm whether the zinc chemically bonds to sulfide and oxide at the same time, X-ray photoelectron spectroscopy (XPS) analysis has been also carried out. The fine spectra of $Zn2p_{3/2}$, O1s, and S2p for each semiconductor were compared. According to the result shown in Fig. 5a, the $Zn2p_{3/2}$ binding energies for ZnO and ZnO_xS_{1-x} were 1020.0 and 1020.8 eV, respectively. In addition, the O1s binding energies for these semiconductors were 529.6 and 530.6 eV (Fig. 5b), respectively. Meanwhile, the peaks of $Zn2p_{3/2}$ and S2p binding energies for ZnO_xS_{1-x} were located at 1020.8 and 161.8 eV, respectively, both shifted to a lower energy side comparing to those for ZnS (Fig. 5a and c). Therefore, it was verified that chemical bonding between zinc and sulfur or oxygen in ZnO_xS_{1-x} was different to that in both ZnS and ZnO. We expected that it has been modified when ZnS and ZnO had been co-precipitated and aged during the preparation process (see Section 2). With the results obtained from the XRD and XPS analyses for a basis, we insist that ZnS and ZnO should organize a solid solution made of an oxysulfide, ZnO_xS_{1-x}.

We have expected that the composite semiconductor, ZnO_xS_{1-x}, would have different characteristic comparing to pure ZnS and ZnO and we gave attention to its application to photocatalysis under visible-light irradiation. Thus, diffuse reflectance spectra (DRS) of ZnS, ZnO, and ZnO_xS_{1-x} were obtained and they are illustrated in Fig. 6. The spectra were plotted as Kubelka–Munk function versus wavelength of light. The plots afford threshold wavelength (λ_{th}) from 360, 397, and 520 nm for ZnS, ZnO, and ZnO_xS_{1-x}, respectively (Table 1). This absorption features indicate that the ZnO_xS_{1-x} has the most predominant absorptivity for visible light among the semiconductors. Compared to pure ZnS and ZnO, the absorptivity of ZnO_xS_{1-x} extended favorably into visible-light region. We are assured that this substantial red-shift of ZnO_xS_{1-x} has been caused by the modified chemical bonding between zinc and oxide or sulfur indicating the formation of solid solution of ZnS and ZnO.

As it is given in Table 1, the calculated band-gap energies from the DRS results of three semiconductors were ca. 3.5, 3.1,
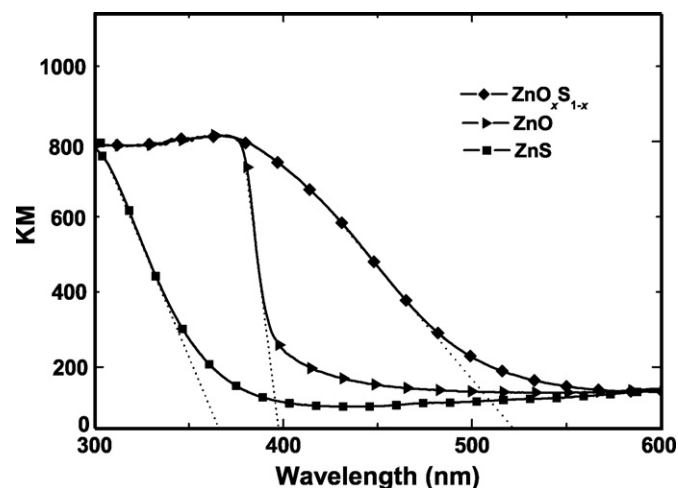
Table 1
Threshold wavelengths and band-gap energies of ZnS, ZnO, and ZnO_xS_{1-x}

	ZnS	ZnO	ZnO_xS_{1-x}
λ_{th} (nm)[a]	360	397	520
Band-gap energy (eV)	3.5	3.1	2.4

[a] Threshold wavelength.

and 2.4 eV for ZnS, ZnO, and ZnO_xS_{1-x}, respectively. The band-gap diminution of ZnO_xS_{1-x} has been caused by the formation of hybrid orbitals in valence band. As it was already mentioned in Section 1, there have been many reports that hybrid orbitals made of an oxynitride [36,43] and an oxysulfide [42] form a stable valence band in a more negative position, thus they cause small band-gap energy. Therefore, we presented schematic band structure of ZnO_xS_{1-x}. ZnS and ZnO exhibit the conduction and valence band edge positions shown in Fig. 7, which have been obtained from empirical calculation [44,45]. Meanwhile, we expected that hybrid orbitals of sulfur and oxygen should be formed in valence band of ZnO_xS_{1-x} since sulfur exists as an anion (S^{2-}) in ZnS and the top of its valence band may be predominantly composed of S3p orbitals because they have higher potential energies than O2p orbitals [21,37,42]. Thus, HOMO level of ZnO_xS_{1-x} has been built up in the range of a more negative potential energy than that of ZnO. In addition, it was assumed that the conduction band position of ZnO_xS_{1-x} had been also transformed by the formation of the solid solution. We expected that the conduction band of ZnO_xS_{1-x} would place between that of ZnS and ZnO since the electronic state of $Zn2p_{3/2}$ orbital in ZnO_xS_{1-x} exhibited intermediate characteristic as shown in Fig. 5a. Consequently, ZnO_xS_{1-x} had small band-gap energy (2.4 eV) and exhibited enhanced absorptivity for visible light (Fig. 6). We assumed that the band structure of ZnO_xS_{1-x} should be composed of the hybrid orbitals indicating an oxysulfide in valence band and Zn3d orbitals in conduction band (Fig. 7). Overall, we insist that the hybrid orbitals consisting of an oxysulfide play an important role in decreasing band-gap energy, therefore the oxysulfide was an active component for visible-light response of the composite semiconductor.

To explore the activities for photocatalytic degradation of Basic Red 2 (1.43×10^{-5} mol L^{-1}), the decolorization test was

Fig. 6. UV–vis diffuse reflectance spectra (DRS) of ZnS, ZnO, and ZnO_xS_{1-x}. The intensities of these spectra were normalized.
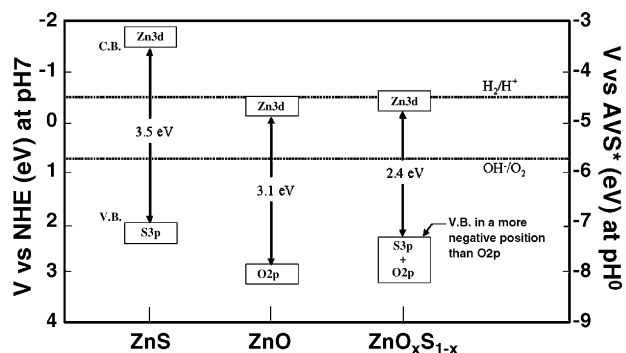

Fig. 7. Calculated energy positions of conduction and valence band edges for ZnS and ZnO [44,45] and schematic band structure of ZnO_xS_{1-x}. *AVS: absolute vacuum scale.
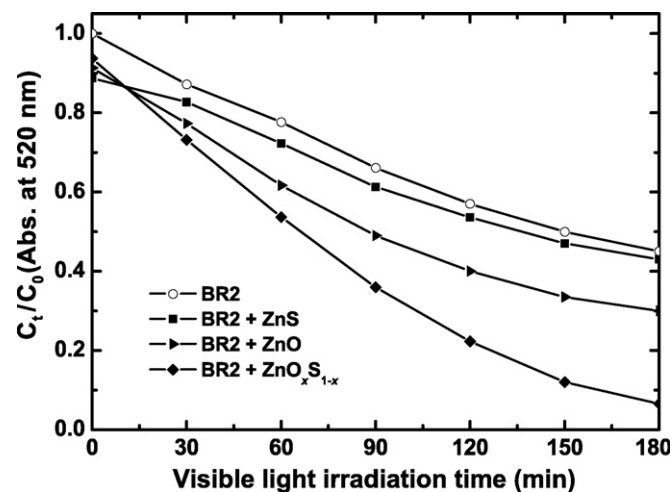
Fig. 8. Photocatalytic activities of ZnS, ZnO, and ZnO_xS_{1-x}. Basic Red 2 concentration = $(1.35 \pm 0.08) \times 10^{-5}$ mol L^{-1}, catalyst amount = 1 g L^{-1}.
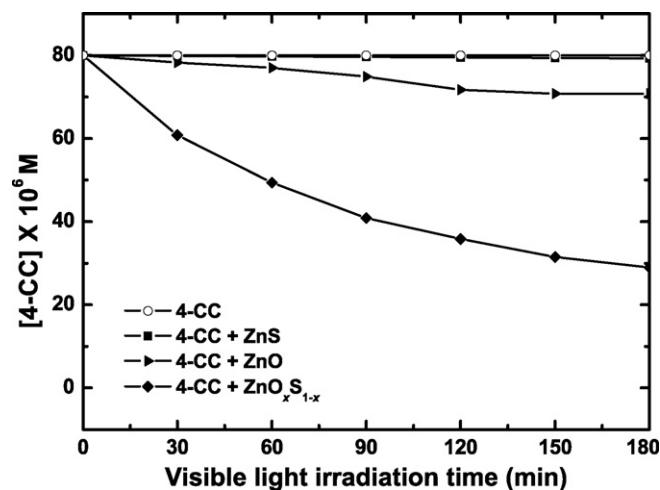

Fig. 9. Photocatalytic activities of ZnS, ZnO, and ZnO_xS_{1-x}. 4-CC concentration = 8×10^{-5} mol L^{-1}, catalyst amount = 1 g L^{-1}.

carried out using artificial visible light ($\lambda > 400$ nm). As it was already mentioned, we simply adopted a cut-off filter for light separation and a UV–vis spectrophotometer for the analysis (see Section 2). Since adsorption of BR2 on the surface of the photocatalysts was detected, mixtures of BR2 and each photocatalyst were stirred for 30 min prior to the irradiation. In the absence and presence of the photocatalysts, BR2 degradation was observed under visible-light irradiation for 180 min (Fig. 8). According to the first-order rate constants, ZnO_xS_{1-x} recorded the highest degradation rate among the photocatalysts (Table 2). However, it was not affirmed that ZnO_xS_{1-x} should have photocatalytic activity under visible-light irradiation since more than 50% of BR2 was also degraded without any photocatalysts as shown in Fig. 8. In addition, the absorption pattern shown in Fig. 1a exhibits that BR2 has the maximum absorption wavelength at 520 nm. Therefore, this result was not enough to confirm the activity of visible-light driven photocatalyst, ZnO_xS_{1-x}. Thus, it was required to choose an additional pollutant being unable to absorb visible light.

According to absorbance spectrum of 4-chlorocatechol (4-CC) shown in Fig. 1b, it absorbs UV light especially below the wavelength of 300 nm. It is an adequate pollutant to estimate activities of visible-light driven photocatalysts since it does not show any absorption peak above the wavelength of 400 nm. The photocatalytic activities for 4-CC degradation of ZnS,

ZnO, and ZnO_xS_{1-x} are presented in Fig. 9. Because 4-CC does not absorb any visible light, no degradation was detected without the photocatalysts. Meanwhile, different degradation pattern emerged when the photocatalysts were used. The photocatalytic activity of ZnO_xS_{1-x} was much superior to that of pure ZnS or ZnO. This was also confirmed by the rate constants of photocatalytic reactions each photocatalyst has been applied (Table 3). As it was indicated, ZnO_xS_{1-x} recorded larger rate constant for 4-CC photodegradation than ZnO and ZnS by ca. 10–100 times. Apparently, this enormous gap should be caused by the enhanced visible-light absorptivity of ZnO_xS_{1-x}. As it was already proven, the composite semiconductor has been generated during the co-precipitation process and this decisively rendered to the band-gap diminution. We insist that an oxysulfide in ZnO_xS_{1-x} should lift HOMO level up, thus decreased band gap (2.4 eV) occurred. This band gap seemed to be narrow enough to absorb visible light and form electron-hole pairs for photocatalysis, effectively.

We are still investigating to find the most appropriate molar ratio between ZnS and ZnO to gain a ZnO_xS_{1-x} composite photocatalyst with optimum visible-light absorptivity and photocatalytic activities for the degradation of organic pollutants under visible-light irradiation. We expect that the ZnO_xS_{1-x} would undergo a change in x value (oxygen to sulfur ratio) depending on the molar ratio and various properties of ZnO_xS_{1-x}, such as band-gap energy, visible-light absorptivity, and photocatalytic activity under visible-light illumination could be also altered, remarkably.

Table 2
First-order rate constants for the photocatalytic degradation of BR2 under visible-light irradiation

Photocatalyst	r^2	k (min^{-1})
w/o[a]	0.99	4.54×10^{-3}
ZnS	0.99	4.29×10^{-3}
ZnO	0.99	6.48×10^{-3}
ZnO_xS_{1-x}	0.98	1.49×10^{-2}

$C_{BR2}^0 = (1.35 \pm 0.08) \times 10^{-5}$ mol L^{-1}.
[a] Photodegradation of BR2 without photocatalyst.

Table 3
First-order rate constants for the photocatalytic degradation of 4-CC under visible-light irradiation

Photocatalyst	r^2	k (min^{-1})
ZnS	1	5.22×10^{-5}
ZnO	0.98	7.59×10^{-4}
ZnO_xS_{1-x}	0.98	5.57×10^{-3}

$C_{4\text{-}CC}^0 = 8 \times 10^{-5}$ mol L^{-1}.

4. Conclusions

The ZnO_xS_{1-x} composite photocatalyst with 1:3 molar ratio was prepared by brief co-precipitation process. It was turned out that ZnS and ZnO composed a solid solution, zincoxysulfide (ZnO_xS_{1-x}). This oxysulfide contributed to the enhanced visible-light absorptivity of ZnO_xS_{1-x} inasmuch as it organized hybrid orbitals consisting of S3p and O2p and valence band of ZnO_xS_{1-x} has been molded in a more negative position. Thus, ZnO_xS_{1-x} exhibited much superior visible-light absorptivity to pure ZnS or ZnO, which have wide band-gap energies, due to band-gap diminution. We verified that the ZnO_xS_{1-x} photocatalyst recorded advanced activities for the degradation of organic pollutants, such as BR2 and 4-CC under visible-light irradiation.

Consequently, it was confirmed that the oxysulfide in the ZnO_xS_{1-x} photocatalyst played a key role in the enhanced visible-light absorptivity and the outstanding activity for the photocatalytic degradation of an organic pollutant under visible-light irradiation.

Acknowledgements

References

[1] S. Sakthivel, M.V. Shankar, M. Palanichamy, B. Arabindoo, D.W. Bahnemann, V. Murugesan, Water Res. 38 (2004) 3001.
[2] A.A. Khodja, T. Sehili, J.-F. Pilichowski, P. Boule, J. Photochem. Photobiol. A 141 (2001) 231.
[3] M. Mrowetz, E. Selli, J. Photochem. Photobiol. A 180 (2006) 15.
[4] C.A.K. Gouvêa, F. Wypych, S.G. Moraes, N. Durán, N. Nagata, P. Peralta-Zamora, Chemosphere 40 (2000) 433.
[5] A.A. Ismail, I.A. Ibrahim, M.S. Ahmed, R.M. Mohamed, H. El-Shall, J. Photochem. Photobiol. 163A (2004) 445.
[6] X.Z. Li, H. Liu, L.F. Cheng, H.J. Tong, Environ. Sci. Technol. 37 (2003) 3989.
[7] Q.X. Dai, H.Y. Xiao, W.S. Li, Y.Q. Na, X.P. Zhou, J. Comb. Chem. 7 (2005) 539.
[8] C. Chen, W. Zhao, J. Li, J. Zhao, H. Hidaka, N. Serpone, Environ. Sci. Technol. 36 (2002) 3604.
[9] S.O. Obare, T. Ito, M.H. Balfour, G.J. Meyer, Nano Lett. 3 (2003) 1151.
[10] A.Y. Nosaka, T. Fujiwara, H. Yagi, H. Akutsu, Y. Nosaka, Langmuir 19 (2003) 1935.
[11] S. Lee, C. Fan, T. Wu, S.L. Anderson, J. Am. Chem. Soc. 126 (2004) 5682.
[12] J.J. Sene, W.A. Zeltner, M.A. Anderson, J. Phys. Chem. B 107 (2003) 1597.
[13] H. Park, W. Choi, J. Phys. Chem. B 107 (2003) 3885.
[14] H.G. Kim, D.W. Hwang, J.S. Lee, J. Am. Chem. Soc. 126 (2004) 8912.
[15] C. Burda, Y. Lou, X. Chen, A.C.S. Samia, J. Stout, J.L. Gole, Nano Lett. 3 (2003) 1049.
[16] J. Premkumar, Chem. Mater. 16 (2004) 3980.
[17] S. Sakthivel, M. Janczarek, H. Kisch, J. Phys. Chem. B 108 (2004) 19384.
[18] M. Takahashi, K. Tsukigi, E. Dorjpalam, Y. Tokuda, T. Yoko, J. Phys. Chem. B 107 (2003) 13455.
[19] H. Kikuchi, M. Kitano, M. Takeuchi, M. Matsuoka, M. Anpo, P.V. Kamat, J. Phys. Chem. B 110 (2006) 5537.
[20] A. Ghicov, J.M. Macak, H. Tsuchiya, J. Kunze, V. Haeublein, L. Frey, P. Schmuki, Nano Lett. 6 (2006) 1080.
[21] I. Tsuji, H. Kato, H. Kobayashi, A. Kudo, J. Am. Chem. Soc. 126 (2004) 13406.
[22] C. Lettmann, K. Hildenbrand, H. Kisch, W. Macyk, W.F. Maier, Appl. Catal. B 32 (2001) 215.
[23] S. Khan, M. Al-Shahry, W.B. Ingler, Science 297 (2002) 5590.
[24] S. Sakthivel, H. Kisch, Angew. Chem. 115 (2003) 5057.
[25] S. Sato, Chem. Phys. Lett. 123 (1986) 126.
[26] R. Asahi, T. Morikawa, T. Ohwaki, A. Aoki, Y. Taga, Science 293 (2001) 269.
[27] H. Irie, Y. Watanabe, K. Hashimoto, J. Phys. Chem. B 107 (2003) 5483.
[28] T. Lindgren, J.M. Mwabora, E. Avendano, J. Jansson, A. Hoel, C.-G. Granqvist, S.-E. Lindquist, J. Phys. Chem. B 107 (2003) 5709.
[29] J.L. Gole, J.D. Stout, C. Burda, Y. Lou, X. Chen, J. Phys. Chem. B 108 (2004) 1230.
[30] O. Diwald, T.L. Thomson, T. Zubkov, Ed.G. Goralski, S.D. Walck, J.T. Yates, J. Phys. Chem. B 108 (2004) 6004.
[31] T. Umebayashi, T. Yamaki, H. Itoh, K. Asai, Appl. Phys. Lett. 81 (2002) 454.
[32] T. Umebayashi, T. Yamaki, S. Tanaka, K. Asai, Chem. Lett. 32 (2003) 330.
[33] T. Ohno, T. Mitsui, M. Matsumura, Chem. Lett. 32 (2003) 364.
[34] A. Kudo, K. Ueda, I. Mikami, Catal. Lett. 53 (1998) 391.
[35] A. Kudo, K. Omori, H. Kato, J. Am. Chem. Soc. 121 (1999) 11459.
[36] M. Hara, G. Hitoki, T. Takata, J.N. Kondo, H. Kobayashi, K. Domen, Catal. Today 78 (2003) 555.
[37] K. Maeda, K. Teramura, T. Takata, M. Hara, N. Saito, K. Toda, Y. Inoue, H. Kobayashi, K. Domen, J. Phys. Chem. B 109 (2005) 20504.
[38] J. Lin, J.C. Yu, D. Lo, S.K. Lam, J. Catal. 183 (1999) 368.
[39] M. Yoshino, M. Kakihana, C.W. Seok, H. Kato, A. Kudo, Chem. Mater. 14 (2002) 3369.
[40] H. Kato, A. Kudo, J. Photochem. Photobiol. A 145 (2001) 129.
[41] A. Harriman, J.M. Thomas, W. Zhou, D.A. Jefferson, J. Solid State Chem. 72 (1988) 126.
[42] A. Ishikawa, T. Takata, J.N. Kondo, M. Hara, H. Kobayashi, K. Domen, J. Am. Chem. Soc. 124 (2002) 13547.
[43] A. Kasahara, N. Nukumizu, T. Takata, J.N. Kondo, M. Hara, H. Kobayash, K. Domen, J. Phys. Chem. B 107 (2003) 791.
[44] Y. Xu, M.A.A. Schoonen, Am. Mineral. 85 (2000) 543.
[45] N. Serpone, P. Maruthamuthu, P. Pichat, E. Pelizzetti, H. Hidaka, J. Photochem. Photobiol. A 85 (1995) 247.